Received May 2003
Revised February 2004
Accepted May 2004

Steady and unsteady thermal analysis of a triple stack cold plate with heat losses

Shiao Lin Beh
Faculty of Engineering and Technology, Multimedia University, Melaka, Malaysia
C.K. Ooi, G.A. Quadir and K.N. Seetharamu
School of Mechanical Engineering, University Sains Malaysia, Seri Ampangan, Penang, Malaysia

Abstract

Purpose – To provide some new and additional data for the design of a triple stack cold plate.

Design/methodology/approach – A detailed finite element formulation for the triple stack cold plate with and without heat losses from the top and bottom surfaces of the stack is presented to determine its performance under steady as well as unsteady conditions. The effects of the number of unit cells, different heat losses as well as the governing dimensionless parameter, M (involving stack dimension, properties of the stack material and the variation in the heat transfer coefficient) on the performance of the stack are investigated. The detailed formulation of the asymptotic waveform evaluation scheme is also given and applied to determine the transient performance of the stack.

Findings – The methods of analysis described are quite simple to use to determine the steady and unsteady performance of the triple stack cold plate under different operating conditions. The heat losses from the top and bottom surfaces of the stack do affect the maximum temperature of the stack and in such case, the assembled stack should be analysed.

Research limitations/implications – The analysis is limited to an incompressible fluid. The effect of varying mass flow rate of the fluid in the stack passages is also not considered.

Practical implications – New and additional generated data will be helpful in the design of cold plates used in the cooling of electronic components.

Originality/value – The asymptotic waveform evaluation scheme is used for the first time to determine the transient performance of the triple stack cold plate under different operating conditions. The results thus obtained are compared well with those found from the finite element analysis (FEM), but the computational effort and time required in the analysis is much small as compared to those required in the FEM analysis.

Keywords Finite element analysis, Heat loss, Cooling, Electronic equipment and components
Paper type Technical paper

Nomenclature

A = cross sectional area perpendicular to the direction of heat conduction, m^2
c = specific heat of the fin material, J/kg °C
h = heat transfer coefficient, W/m^2K
k = thermal conductivity of the fin material, W/m °C
M = hPB^2/kA, a non-dimensional stack parameter
P = perimeter of the surface where convection takes place, m
$\tilde{Q}$ = Heat loading on the right exterior plate/Heat loading on the left exterior plate = Q_{TR}/Q_{TL}
T = temperature of the fin at a given location, °C
T_∞ = ambient temperature, °C

International Journal for Numerical Methods in Heat & Fluid Flow
Vol. 15 No. 1, 2005
pp. 96-112

0961-5539
DOI 10.1108/09615530510571976

t = time, s
X = x/B, where B is the reference dimension, m
x = distance measured from the base of a fin, m
ρ = density of the fin material, kg/m^3
τ = $kt/\rho cB^2$, a non-dimensional time
θ = $kA(T - T_\infty)/Q_{TI}B$, a non-dimensional temperature
θ_i, θ_j = dimensionless temperature at nodes i and j, respectively
θ_{it}, θ_{jt} = temperature at a node for two time intervals represented by it and jt

Introduction

Electronic components mounted on the printed circuit board are cooled using cold plates which consist of repeated arrays of rectangular fins, attached between two exterior plates. Fluid passes through the spaces between the fins to help increase the rate of heat transfer from the fin. A triple stack cold plate has two splitter plates between the two exterior plates. Kern and Kraus (1972) analysed the single stack and double stack cold plates with heat input on one side, as well as on both sides of the cold plates. Kraus *et al.* (1978), for arrays of single fin, showed that the condition of heat flow and excess temperature at any point on a fin are influenced by similar conditions at the fin base.

A limited steady-state analysis of a double stack cold plate, as shown in Figure 1, was reported by Pieper and Kraus (1995) and Kraus and Pieper (1995). Their analyses were valid only if the imbalance in heat loading at the cover plate exterior surfaces was sufficient to generate an adiabatic point somewhere along either the left hand fin or the right hand fin in the structure. The range in the imbalance in thermal loading for which such an adiabatic point did not exist was established to be greater than zero. Pieper and Kraus (1998) extended their analysis for a double stack, forced cooled cold plates to cover all regimes of asymmetric loading, including the previously ignored operating regime in which neither of the fins connecting exterior surfaces to splitter plates had an adiabatic point. They considered the entire structure to be composed of a large number of repeating sections called the unit cells as identified within the box shown in Figure 1. End effects were ignored for large number of such repeating sections. Identical thermal conditions were implied on each cell of the structure. The overall performance of the double stack cold plate was approximately predicted by appropriately scaling the performance analysis of the basic repeating section. They also showed that, disregarding fluid movement considerations, the double stack cold plate could keep the electronic package cooler than the corresponding single stack design having the same volume. However, their results were limited to the given stack dimensions only.

The objective of this paper is to present the steady-state performance of a triple stack cold plate with heat losses from the top and bottom surfaces of the stack with varying number of unit cells (NUC) using finite element method. Further, a fast transient asymptotic waveform evaluation (AWE) method is applied to determine the transient behaviour of the triple stack cold plate and the results thus obtained are compared with those obtained by the finite element method.

The governing equation and finite element formulation

A stack is considered as a combination of fins connected together. A simple one-dimensional fin theory is then applied to the stack under investigation (Quadir *et al.* 2002).

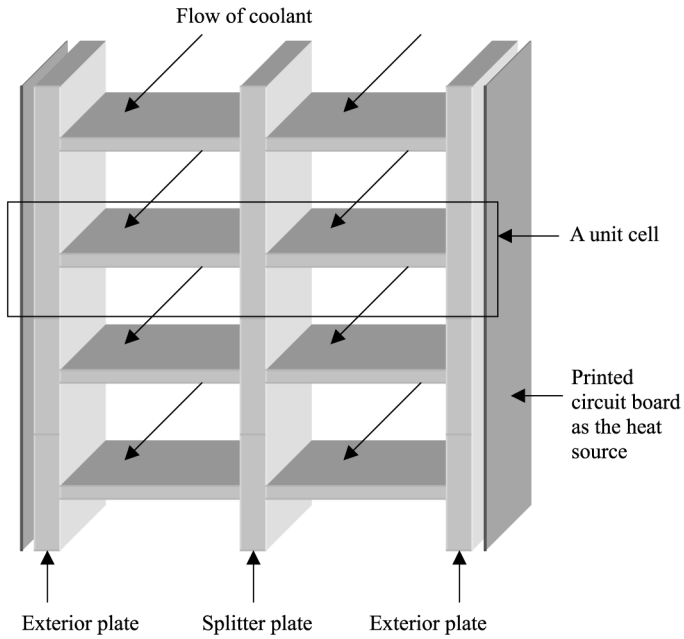

Figure 1.
A double stack cold plate with unit cell marked

The governing equation under a transient condition for a one-dimensional fin with conduction and forced convection is given as follows:

$$kA\frac{\partial^2 T}{\partial x^2} - hP(T - T_\infty) = c\rho A\frac{\partial T}{\partial t} \tag{1}$$

As a generalisation, using the dimensionless parameters $\tilde{Q}$, θ, X, M and τ, as defined in the nomenclature, equation (1) becomes:

$$\frac{\partial^2 \theta}{\partial X^2} - M\theta = \frac{\partial \theta}{\partial \tau} \tag{2}$$

M is the governing parameter in the analysis that takes into account the variation in h (free convection, mixed convection and forced convection including the developing flow), the variation in k (different fin materials), geometric factor (A/P ratio of the flow passage) and finally, the distance between the exterior plates. Thus, the introduction of the parameter M does not restrict the present analysis to a particular set of geometry.

The variation of temperature along the fin is assumed to be linear as:

$$\theta = [N]\{\theta\} \tag{3}$$

where $[N]$ is the shape function and given by:

$$[N] = \begin{bmatrix} 1 - X & X \end{bmatrix}, \tag{4}$$

and

$$\{\theta\} = \begin{Bmatrix} \theta_i \\ \theta_j \end{Bmatrix} \tag{5}$$

By using Galerkin's method, as explained in Segerlind (1984) and Lewis *et al.* (1996), the finite element formulation of equation (2) is obtained as:

$$[C]\left\{\frac{\mathrm{d}\theta}{\mathrm{d}\tau}\right\} + [K]\{\theta\} = 0 \tag{6}$$

where

$$[C] = \frac{1}{6}\begin{bmatrix} 2 & 1 \\ 1 & 2 \end{bmatrix} \tag{7}$$

$$[K] = \begin{bmatrix} 1 & -1 \\ -1 & 1 \end{bmatrix} + \frac{M}{6}\begin{bmatrix} 2 & 1 \\ 1 & 2 \end{bmatrix} \tag{8}$$

Equation (6) is a transient heat conduction equation. To solve this equation using FEM, the temperature variation with time is assumed to be linear and is represented as:

$$\{\theta\} = N_{it}\{\theta_{it}\} + N_{jt}\{\theta_{jt}\} \tag{9}$$

where

$$N_{it} = 1 - \frac{\tau}{\Delta\tau} \text{ and } N_{jt} = \frac{\tau}{\Delta\tau} \tag{10}$$

where $\Delta\tau$ is the non-dimensional time step.

Galerkin's method is applied in the time domain here, to obtain the time stepping scheme as:

$$\left(\frac{[C]}{2\Delta\tau} + \frac{[K]}{6}\right)\{\theta_{jt}\} = \left(\frac{[C]}{2\Delta\tau} - \frac{[K]}{3}\right)\{\theta_{it}\} \tag{11}$$

Equation (11) is used to find the temperature distribution $\{\theta_{jt}\}$ at a new time step from the known temperature distribution $\{\theta_{it}\}$. The iteration stops when the temperature between the two time steps does not change by more than 1.0×10^{-6}. The above theory can be applied to different cases, e.g. fin array, single stack cold plate, double stack cold plate and triple stack cold plate. The assembly of the element matrices for each case is to be carried out similar to that as explained in Segerlind (1984).

AWE formulation

Laplace transform of equation (6) is given as follows:

$$[C]\{s\theta(s) - \theta_0\} + [K]\{\theta(s)\} = \{b\} \tag{12}$$

where θ_0 refers to the initial condition of the system, and $\{b\}$ the load vector.

Subsequent steps treat the boundary conditions and initial conditions in two separate solutions, which are then combined to give the total solution. This is

equivalent to solving a control system, where the response of the system is represented by a combination of two independent responses, namely zero state response (ZSR) and zero input response (ZIR).

The ZSR is evaluated by treating the initial condition of the system as zero. In terms of the present analysis, this means the initial temperature of the cold plate is equal to the ambient temperature. Therefore, equation (12) is simplified as follows.

$$(s[C] + [K])\{\theta(s)\} = \{b\} \tag{13}$$

Next, the Taylor series expansion of $\theta(s)$ about $s = 0$ is evaluated in order to obtain the moments M_n which are defined in the following equation.

$$\theta(s) = \theta(0) + \frac{\theta'(0)s}{1!} + \frac{\theta''(0)s^2}{2!} + \frac{\theta'''(0)s^3}{3!} + \cdots = \sum_{n=0}^{\infty} M_n s^n \tag{14}$$

where

$$M_n = \frac{\theta^n(0)}{n!}.$$

Also, when $s = 0$, equation (13) becomes $[K]\{\theta(0)\} = \{b\}$, and equation (14) becomes $\{\theta(0)\} = M_0$. These two equations are combined to become $M_0 = [K]^{-1}\{b\}$. Thus, the first moment M_0 for ZSR is obtained.

In order to evaluate the second moment M_1, equation (12) is differentiated once with respect to s, then setting $s = 0$, we obtain $[K]\{\theta'(0)\} + [C]\{\theta(0)\} = 0$. Also, from equation (14), when $n = 1$, $M_1 = \{\theta'(0)\}$. Thus, the second moment is obtained as $[K]M_1 = -[C]M_0$. Based on the same argument, the nth moment M_n can be obtained from a general formula: $[K]M_n = -[C]M_{n-1}$.

The ZIR is evaluated by treating the forcing function of the system as zero. In terms of the present analysis, this means the heat loading of the cold plate is equal to zero. Therefore, equation (12) is simplified as follows.

$$(s[C] + [K])\{\theta(s)\} - [C]\{\theta_0\} = 0 \tag{15}$$

Next, the Taylor series expansion of $\theta(s)$ about $s = 0$ for ZIR is evaluated to obtain the moments M_n as defined in equation (14). Also, when $s = 0$, equation (15) becomes $[K]\{\theta(0)\} = [C]\{\theta_0\}$, and equation (14) becomes $\{\theta(0)\} = M_0$. These two equations are combined to get $M_0 = [K]^{-1}[C]\{\theta_0\}$. Thus, the first moment M_0 for ZIR is obtained.

In order to evaluate the second moment M_1, equation (15) is differentiated once with respect to s, then setting $s = 0$, we obtain $[K]\{\theta'(0)\} + [C]\{\theta(0)\} = 0$. Also, from equation (14), when $n = 1$, $M_1 = \{\theta'(0)\}$. Thus, the second moment is obtained as $[K]M_1 = -[C]M_0$. Based on the same argument, the nth moment M_n can be obtained from a general formula: $[K]M_n = -[C]M_{n-1}$. M_n is the nth moment of all nodes. Since the response of only one node is of our interest, we extract the moments of that node for further calculations, instead of working with the moments of all nodes. Let m_n be the ith entry in vector M_n. m_n represents the moments generated from node i (the node of our interest). Thus, an equation similar to equation (14) can be written to represent the response of one particular node of interest, as follows:

$$\theta(s) = m_0 + m_1 s + m_1 s^2 + \cdots + m_{2q-1} s^{2q-1} = \sum_{n=0}^{2q-1} m_n s^n \tag{16}$$

Equation (16) must be evaluated twice for ZIR and ZSR separately. In equation (16), the series is finite from 0 to the $(2q-1)$th moment. AWE matches these moments to a reduced order model by using Padé approximation up to q number of moments only, which is strictly a proper rational function, as given by:

$$\theta(s) = \frac{b_0 + b_1 s + b_2 s^2 + \cdots + b_{q-1} s^{q-1}}{1 + a_1 s + a_2 s^2 + \cdots + a_q s^q} \tag{17}$$

Therefore, equations (16) and (17) are combined to obtain:

$$m_0 + m_1 s + m_1 s^2 + \cdots + m_{2q-1} s^{2q-1} = \frac{b_0 + b_1 s + b_2 s^2 + \cdots + b_{q-1} s^{q-1}}{1 + a_1 s + a_2 s^2 + \cdots + a_q s^q} \tag{18}$$

After cross-multiplication, the coefficients of s on the left and right hand side are equated. Thus, a set of linear algebraic equations yields :

$$\begin{gathered}
m_0 a_q + m_1 a_{q-1} + m_2 a_{q-2} + \cdots + m_{q-1} a_1 + m_q = 0 \\
m_1 a_q + m_2 a_{q-1} + m_3 a_{q-2} + \cdots + m_q a_1 + m_{q+1} = 0 \\
m_2 a_q + m_3 a_{q-1} + m_4 a_{q-2} + \cdots + m_{q+1} a_1 + m_{q+2} = 0 \\
\vdots \\
m_{q-1} a_q + m_q a_{q-1} + m_{q+1} a_{q-2} + \cdots + m_{2q-2} a_1 + m_{2q-1} = 0
\end{gathered} \tag{19}$$

Equation (19) can be written in the following matrix form:

$$\begin{bmatrix}
m_0 & m_1 & m_2 & \ldots & m_{q-1} \\
m_1 & m_2 & m_3 & \ldots & m_q \\
m_2 & m_3 & m_4 & \ldots & m_{q+1} \\
\vdots & \vdots & \vdots & \cdots & \vdots \\
m_{q-1} & m_q & m_{q+1} & \ldots & m_{2q-2}
\end{bmatrix}
\begin{Bmatrix}
a_q \\ a_{q-1} \\ a_{q-2} \\ \vdots \\ a_1
\end{Bmatrix}
= -
\begin{Bmatrix}
m_q \\ m_{q+1} \\ m_{q+2} \\ \vdots \\ m_{2q-1}
\end{Bmatrix} \tag{20}$$

Equation (20) is solved for a s, which are then used to find the roots p by the following equation:

$$\sum_{i=0}^{q} a_i p^i = 0, \quad \text{where } a_0 = 1 \tag{21}$$

The roots are then assembled in the following matrix in order to find the residues k.

$$\begin{bmatrix} p_1^{-1} & p_2^{-1} & p_3^{-1} & \cdots & p_q^{-1} \\ p_1^{-2} & p_2^{-2} & p_3^{-2} & \cdots & p_q^{-2} \\ p_1^{-3} & p_2^{-3} & p_3^{-3} & \cdots & p_q^{-3} \\ \vdots & \vdots & \vdots & \cdots & \vdots \\ p_1^{-q} & p_2^{-q} & p_3^{-q} & \cdots & p_q^{-q} \end{bmatrix} \begin{Bmatrix} k_1 \\ k_2 \\ k_3 \\ \vdots \\ k_q \end{Bmatrix} = - \begin{Bmatrix} m_0 \\ m_1 \\ m_2 \\ \vdots \\ m_{q-1} \end{Bmatrix} \tag{22}$$

The poles and residues are then assembled in equation (23), which represents the reduced order approximation. $I(s)$ depends on the nature of the input, e.g. it is equal to 1 for a step input.

$$\theta(s) = \sum_{n=1}^{q} \frac{k_n}{s - p_n} I(s). \tag{23}$$

For each response, the corresponding poles and residues are evaluated and then the total response is evaluated by simply adding the solutions of both ZSR and ZIR for a particular nature of the input. Equation (24) shows the total response in time domain for a step input after performing the inverse Laplace transform where the first summation term represents the solution for ZSR, while the second represents the solution for ZIR.

$$\theta(\tau) = \sum_{i=0}^{q} \frac{k_i}{p_i} (\exp(p_i \tau) - 1) + \sum_{i=0}^{q} k_i \exp(p_i \tau). \tag{24}$$

Validation

The present approach was applied to the case of a rectangular fin array for which solutions are given by Mikhailov and Ozisik (1981). The case of a fin array is taken here because cold plates consist of repeated arrays of rectangular fins between two exterior plates. It is to be noted that Mikhailov and Ozisik (1981) modelled a fin array using a linear combination of two fundamental solutions to the governing differential equation for the one-dimensional steady-state problem. However, in the present analysis each fin can be considered to have more than one element. Thus, the present finite element analysis is more general and can be used for longer fins as well. The results are reported by Beh *et al.* (2001) and found to be in good agreement with those of Mikhailov and Ozisik (1981). This exercise showed that the present approach is valid for the analysis of fin arrays.

The present analysis was also applied to analyse single stack and double stack cold plates, the details of which may be found in Quadir *et al.* (2002 2003). It may be mentioned here that they analysed first a single unit cell being considered as the representative of the whole stack with no heat losses from the top and bottom surfaces of the stack. The steady-state results obtained by them using the present analysis were compared with those of Pieper and Kraus (1998) and found to be in good agreement. Thus, the present methodology was validated against the single and double stack cold plate results available in the literature.

Triple stack cold plate

Since the present methodology is valid for analyzing single and double stack cold plates, the same methodology is extended to a triple stack cold plate to analyse its performance under the same boundary conditions. A single unit cell, being the repeating segments of the triple stack, is considered first. The analysis of this single unit cell is carried out under the same operating conditions as given by Pieper and Kraus (1998) for single and double stack cold plates. Next, different NUC are considered and analysed after having assembled them together vertically with and without heat losses from the top and bottom of the assembled unit.

Single unit cell analysis

Figure 2(a) shows the geometry of a single unit cell of a triple stack cold plate. The discretised single unit cell used for the finite element analysis is shown in Figure 2(b). In this case, the global matrix is a 12×12 matrix as there are 11 elements and 12 nodes. The same heat loadings on the left and right exterior plates are taken as in the case of the analysis of a single unit cell in the single and double stack cold plates.

(a) Geometry of a unit cell of a triple stack cold plate

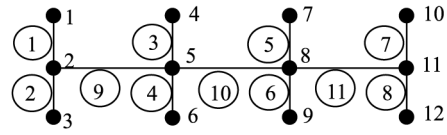

(b) Finite element representation of the unit cell

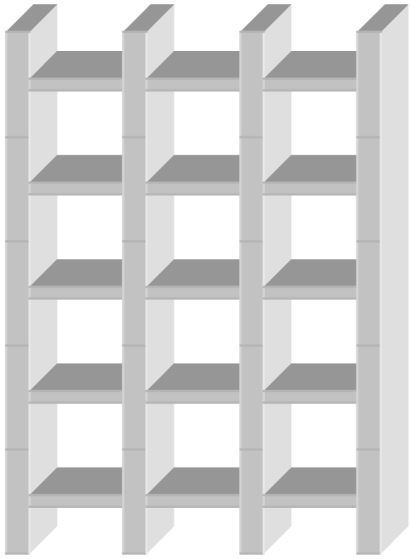

(c) Geometry of the assembly of 5 unit cells

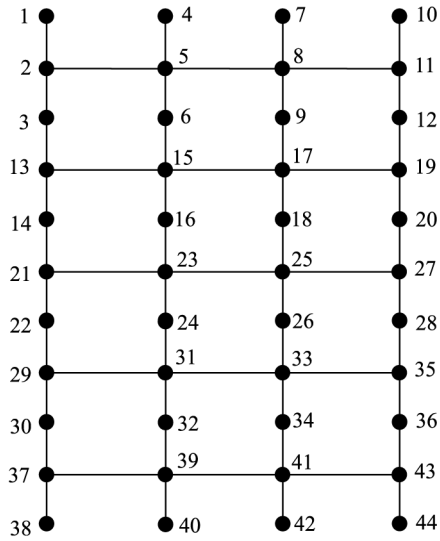

(d) Finite element representation of the assembly of 5 unit cells

Figure 2.

The steady-state results obtained for $M = 0.55$ (same value as given by Pieper and Kraus (1998)) are then plotted in Figure 3 in terms of θ_l and θ_r representing the maximum temperature on the left and right exterior plate, respectively. Generally, the pattern of the curves is similar to that of the single and double stack cold plates (Quadir *et al.*, 2002, 2003). In addition, temperature level of a triple stack cold plate is the lowest among the single, double and triple stack cold plates for the same operating conditions.

Analysis of stack with varying NUC

Analysis of the assembly of different NUC for a triple stack cold plate with and without heat losses is presented as follows. For this, unit cells of a triple stack cold plate are assembled in the vertical direction as shown in Figure 2(c) for five unit cells. Figure 2(d) shows the discretisation of the assembled five unit cells. In order to see the effect of varying NUC on the performance of the triple stack cold plate, several values of NUC are employed during the analysis.

Figure 4 shows different curves of the steady-state temperature distribution at the left exterior plate for $M = 0.55$, NUC = 1, 5, 20, 50 and 100 with heat loss from both ends equals 0, 0.1 and 0.2 and $\tilde{Q} = 1$. It is observed from Figure 4 that when there is no heat loss from both the ends, the steady-state temperature distribution is uniform throughout irrespective of the NUC as shown by the curves $(HL0)_1$, $(HL0)_5$, $(HL0)_{20}$, $(HL0)_{50}$ and $(HL0)_{100}$. In these notations, HL stands for heat loss; 0, 1 and 2 stand for zero, 10 and 20 per cent heat loss; and the subscripts 1, 5, 20, 50 and 100 stand for the number of unit cells being assembled together to form the stack. For the heat loss of 0.1, the maximum temperature θ_l obtained for NUC = 1 drops as compared to the earlier case (zero heat loss) as can be observed from the curve $(HL1)_1$. For NUC = 5 and HL = 0.1, Figure 4 shows that there is not much difference in θ_l as compared to that obtained for NUC = 1 and HL = 0.1 (curves $(HL1)_1$ and $(HL1)_5$). When calculations are carried out for an increased heat loss of 0.2, the trend observed is the same. When NUC = 20, the value of θ_l is higher than that obtained for NUC = 1 or 5 when the above two heat losses are considered. Similar behaviour is observed when NUC is increased to 50. Figure 4 also shows clearly the symmetrical temperature profile and

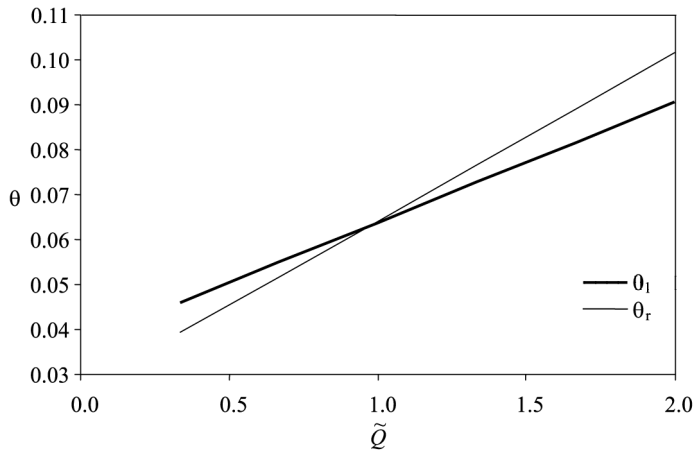

Figure 3.
Dimensionless maximum temperature variation on the left and right exterior plate against heat loading from a single unit cell analysis

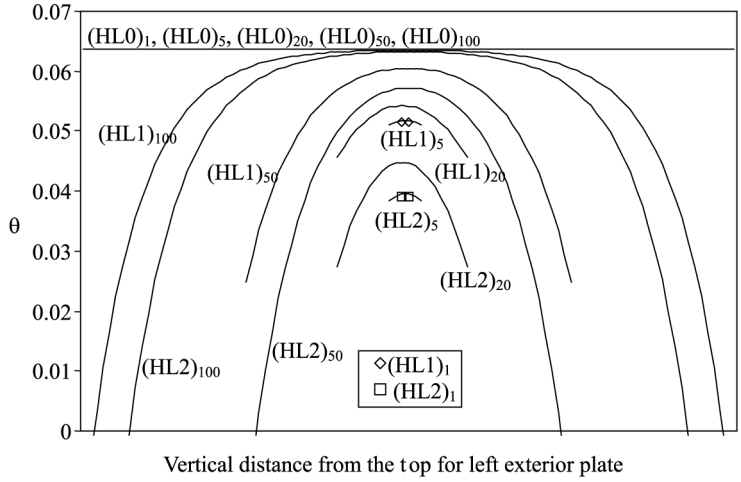

Figure 4.
Temperature distribution at the left exterior plate for various NUC, $\tilde{Q} = 1$ and different heat losses

the lower temperatures at the ends, when the heat loss is considered, by the different curves. However, the temperatures of the near middle cells obtained for NUC = 100 and HL = 0.1 and 0.2 are closer to those obtained for the case with no heat loss as can be seen from the curves $(HL1)_{100}$, $(HL2)_{100}$, $(HL0)_1$, $(HL0)_5$, . . .$(HL0)_{100}$. Furthermore, the curves $(HL1)_{100}$ and $(HL2)_{100}$ representing the temperature variation along the left exterior plate for two different heat losses are very close to each other near the middle cells and differ only at other locations, as expected. Thus, for a triple stack cold plate, it can be concluded that for large NUC (>100) and heat loss being considered, the analysis of a single unit cell without heat loss is adequate to get the temperature distribution near the middle cell or θ_l, which will be helpful to determine whether the maximum temperature limit θ_{max} has been achieved or not. Similar curves for other heat loadings may be drawn to show the steady-state temperature distribution at the right exterior plate as well. The above analysis also shows that a single unit cell analysis with heat loss does not represent the conditions of the middle cell of a stack having any number of repeating segments of unit cell.

Figure 5 shows the steady-state temperature distribution of the right and left exterior plates of the stack ($M = 0.55$) for two values of NUC (20 and 100) under three different heat loadings ($\tilde{Q} = 0.33$, 1 and 2) for a fixed heat loss of 0.2. Based upon the discussion of Figure 4, it may be mentioned here that all the results presented for NUC = 100 for any heat loading give the maximum temperature limit which the stack under investigation will attain irrespective of the heat losses from the top and bottom surfaces of the stack. It may be seen from Figure 5 that the temperature distribution along the right exterior plate at fixed values of NUC and heat loss is the same as that on the left exterior plate when $\tilde{Q} = 1$. The temperature distribution for this equal heat loading ($\tilde{Q} = 1$) for NUC = 100 is clearly shown to be higher than that at NUC = 20 for the same heat loading. When $\tilde{Q}$ is less than 1, the left exterior plate has temperature levels higher than those of right exterior plate for both NUCs as expected. Similarly, when $\tilde{Q}$ is greater than 1, the opposite behaviour in the temperature distribution on the exterior plates is distinctly shown in Figure 5 for $\tilde{Q} = 2$.

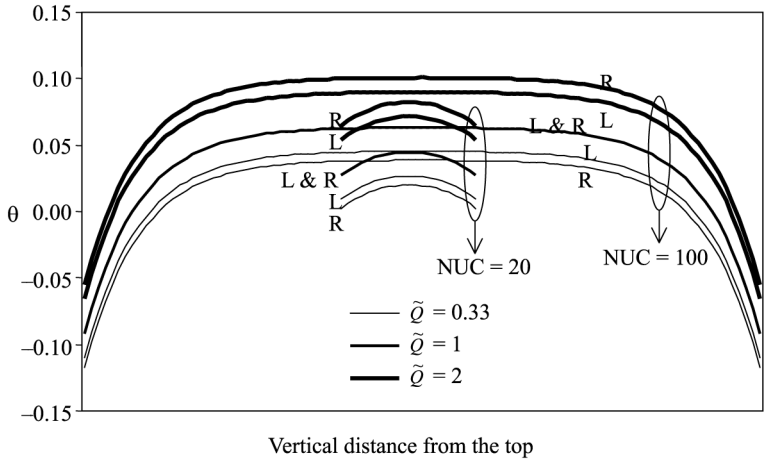

Figure 5.
Temperature distribution at the left and right exterior plate for different $\tilde{Q}$, heat loss = 0.2 and NUC = 20 and 100

The steady-state temperature distributions along the horizontal fin of the middle unit cell for different NUC and different heat loadings $\tilde{Q}$ are shown in Figure 6 where $M = 0.55$ and heat loss = 0.2. Results of the analysis of a single unit cell with zero heat loss for all heat loadings considered are also shown in this figure. The temperature distribution for $\tilde{Q} = 1$ is clearly observed to be symmetric in Figure 6. When $\tilde{Q} = 0.33$, the temperatures at the right nodes are lower than those at the left nodes, which is expected, and this trend is reversed for $\tilde{Q} = 2$. It is also noticed that when $\tilde{Q} = 2$, the second node from the left exterior plate has the lowest temperature among the four nodes along the horizontal fin. It is seen from Figure 6 that the temperature distribution for any heat loading at higher NUC approaches that distribution that is obtained from the analysis of a single unit cell without heat loss at that heat loading. This shows that for NUC $\geq$ 100, the effect of heat loss does not affect the temperature of the cells at or near the middle unit cell.

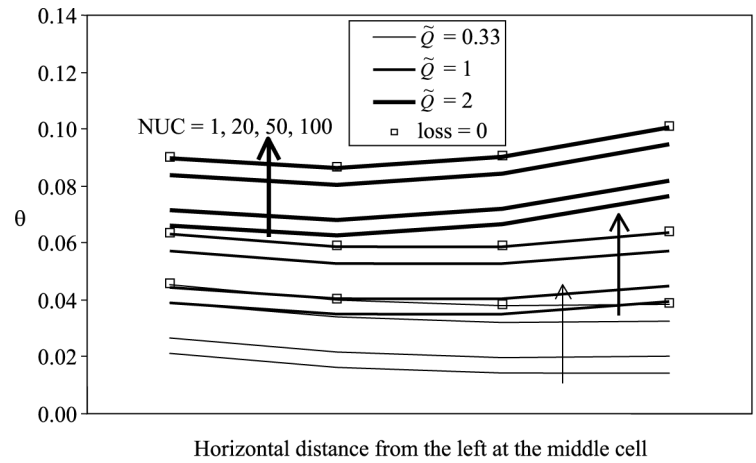

Figure 6.
Temperature distribution along the horizontal fin at the middle of the assembled stack for different heat loadings with different NUC and heat loss = 0.2

Next, a generalized behaviour of the triple stack cold plate is presented by analyzing it for different values of M at different NUC and with and without heat losses from the top and bottom surfaces of the assembled stack. The steady-state results are plotted in terms of the maximum dimensionless temperature obtained either on the left or the right exterior plate depending on the value of $\tilde{Q}$ as shown in Figure 7 when the heat loss = 0.2. Calculations are also carried out for no heat loss and the results are plotted in the same figure for the different heat loadings considered. Thus, Figure 7 shows a generalized performance curve of a triple stack cold plate for $\tilde{Q} = 0.33$, 1 and 2 with heat loss = 0 and 0.2. It is observed from this figure that the θ_{max} obtained for the heat loading $\tilde{Q} = 2$ and NUC = 100 is highest amongst the values obtained for other heat loadings for all the values of $0.25 < M < 2$. Furthermore, the difference between the values of θ_{max} for different values of $\tilde{Q}$ is quite large at lower values of M. However, this difference reduces considerably for $M > 0.5$. It is also noticed from Figure 7 that for $\tilde{Q} = 2$ and NUC = 50, θ_{max} values for $M > 1.0$ coincide with those calculated for zero heat loss as well as with those obtained with NUC = 100 for that heat loading. Similar observation is noticed from the lower curves for $\tilde{Q} = 1$, but beyond a slightly higher value of M as compared to that established for $\tilde{Q} = 2$. This suggests that for values of $M > 1.5$ and even with a heat loss of 0.2, the same results can be obtained from the analysis of a single unit cell without heat loss when NUC exceeds 50.

Figure 8 shows the steady-state temperature distribution at the left and right exterior plates for the heat loading $\tilde{Q} = 0.33$ when the heat loss from the top of the assembled unit (NUC = 20) is different from that of the bottom. Calculated results shown in this figure consider a constant heat loss from the top as 0.2, while heat loss from the bottom varies from 0 to 0.2. The symmetric temperature distribution about the middle of the stack is clearly shown in Figure 8 when the heat losses at both the ends are the same (i.e. 0.2, 0.2). Furthermore, the temperature drop at the top of the cold

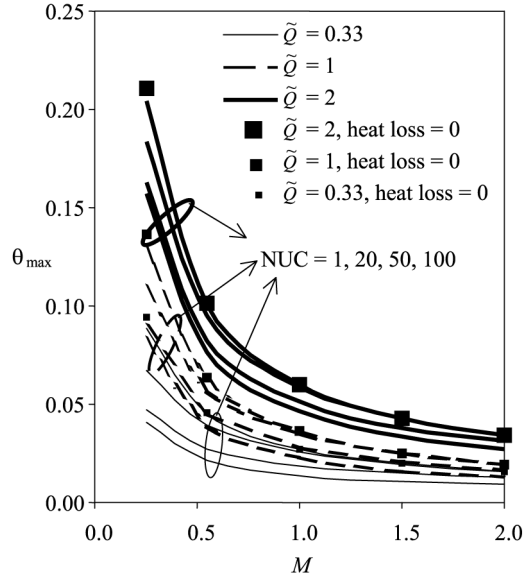

Figure 7.
Dimensionless maximum temperature variation against M for different NUC and for $\tilde{Q} = 0.33$, 1 and 2

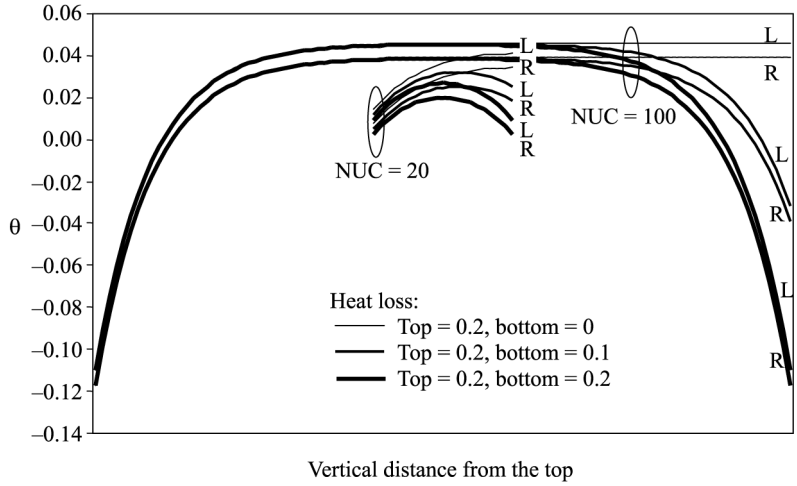

Figure 8.
Temperature distribution at the left and right exterior plates for different heat losses for $\tilde{Q} = 0.33$ and NUC = 20 and 100

plate is more than that at the bottom when the heat loss from the top is larger than that from the bottom.

Comparison of FEM transient results with those from AWE scheme

All the above discussions made are in terms of the steady-state results. The transient behaviour for various working conditions for the triple stack cold plate using the finite element method and the fast transient AWE scheme is discussed below.

Figure 9 shows the comparison of the results obtained by FEM with those from AWE, for the variation of the maximum temperature of the cold plate with respect to time. In this figure the heat loading is unity, heat losses from the upper and lower surfaces of the stack are neglected, and the number of unit cells considered is 100. The three curves using AWE are produced using different number of moments (q) of 2,

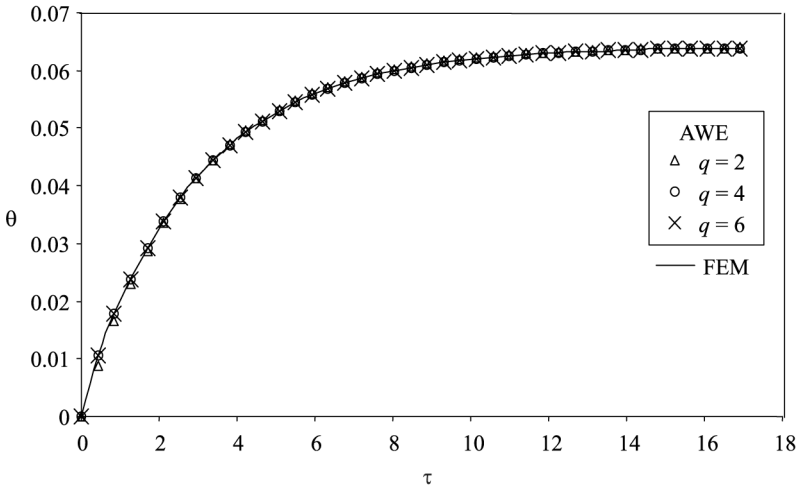

Figure 9.
Comparison between FEM and AWE results for maximum temperature variation for M = 0.55, loss = 0, $\tilde{Q} = 1$ and NUC = 100

4 and 6, respectively. Figure 9 clearly shows that the results using AWE are almost identical to the results using FEM. Slight differences between the two methods are observed when the number of moments is 2. When the number of moments is 4 or 6, it exactly coincides with the FEM solutions.

Figure 10 is a magnified version of Figure 9 for the initial stages of time represented by $\tau = 0 - 1$. This figure clearly demonstrates the differences between the curves using AWE during the initial stages, especially for $q = 2$. However, the difference gets smaller as time progresses, and finally, the curve approaches other curves for higher number of moments $q = 4$ and 6. It can also be seen from this figure that the curves for $q = 4$ and 6 are very close to the curve obtained by using FEM even during the initial stages of time.

Figure 11 shows the effect of the governing parameter M on the maximum temperature of the stack while other parameter such as heat loading is still unity and NUC = 100. The results in this figure correspond to heat loss of 0.2. When M increases, the maximum temperature decreases, as expected. But the time taken to reach the steady-state reduces considerably. This is because a large value of M implies a high value of heat transfer coefficient, which means more heat is transferred from the cold plate to the coolant more quickly. Figure 11 also shows that the results using AWE are close to the results using FEM.

Figure 12 shows the effect of non-uniform heat loadings on the maximum temperature of the cold plate. The results in this figure are shown for a fixed value of M (0.55) with no heat loss and NUC = 100. It is obvious that when heat loading increases, the maximum temperature also increases. It is also observed that the non-uniform heat loading does not change the time taken to reach the steady-state. As before, results using AWE are close to the results using FEM.

Figure 13 shows the comparison of the CPU time for AWE scheme and FEM to solve the stack problem of M = 0.55 for unit heat loading, when different NUC is considered in the analysis. The data are obtained by running the simulation in a Pentium IV 1.4 GHz computer. It can be seen from this figure that FEM needs more time compared to the AWE scheme for all values of NUC. It is also obvious that AWE is at least ten times faster than FEM.

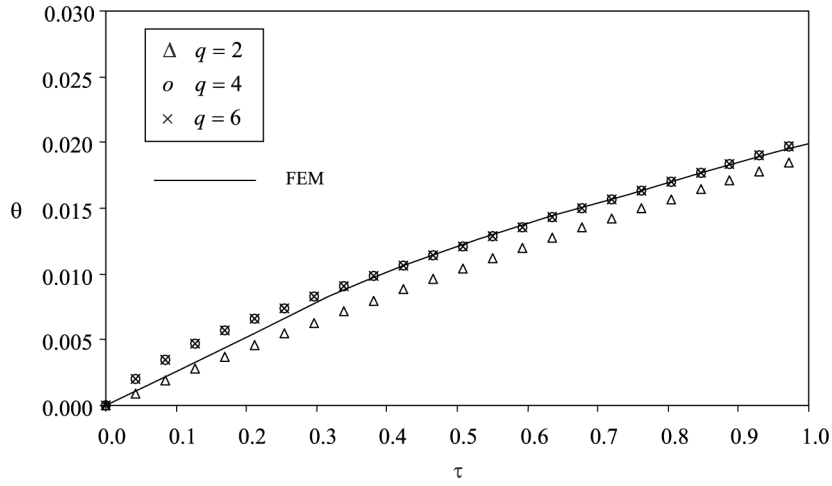

Figure 10.
Magnification of Figure 9 to show the variation of θ in the early period of time for different values of moments q

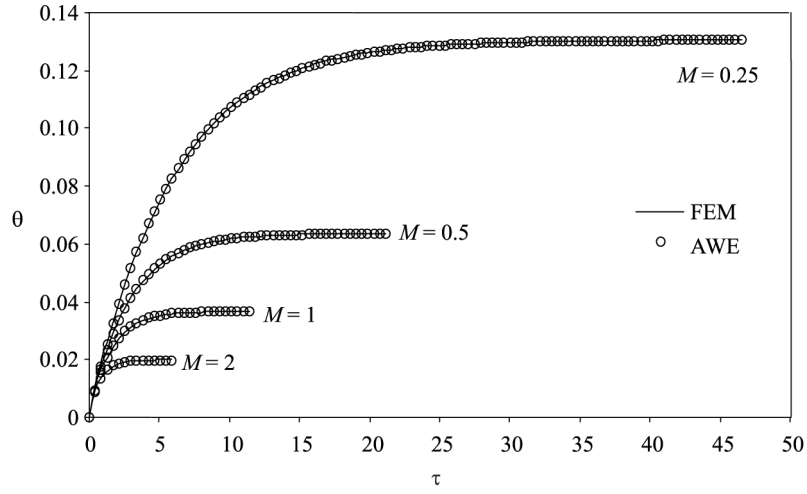

Figure 11.
Comparison of FEM and AWE results of maximum temperature variation for different values of M for loss = 0.2, $\tilde{Q} = 1$ and NUC = 100

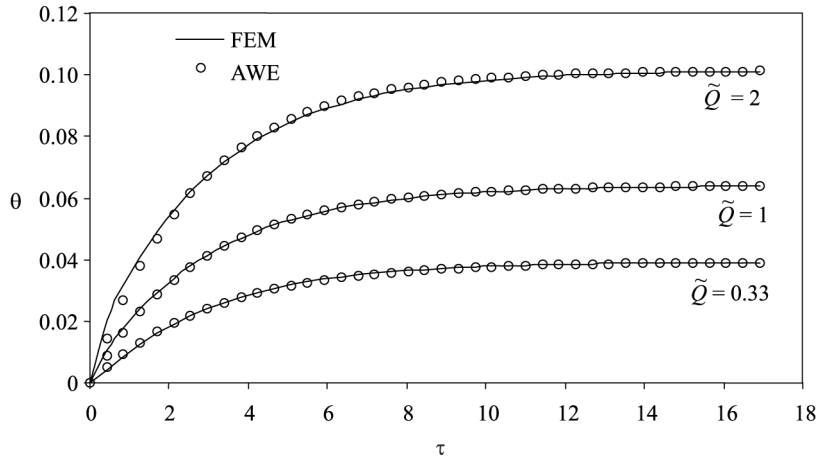

Figure 12.
Comparison between the FEM and AWE results for maximum temperature variation under different values of heat loadings for loss = 0 and NUC = 100

Conclusions

The finite element method is used to analyse a triple stack cold plate in steady and transient conditions as well. A single one-dimensional fin theory is applied to the discretised elements in the above analysis. First, a single unit cell of the stack is analysed with and without heat losses from its top and bottom surfaces for different heat loadings at the exterior plates. Next, the analysis is carried out for an assembly of different NUC under the same boundary conditions as imposed for a single unit cell. Furthermore, the results of the stack analysis for different values of M, a dimensionless parameter involving dimension, properties of the stack material and h are also presented which will be helpful in the design of cold plates used for the cooling of electronic systems. The transient performance is further evaluated using the AWE

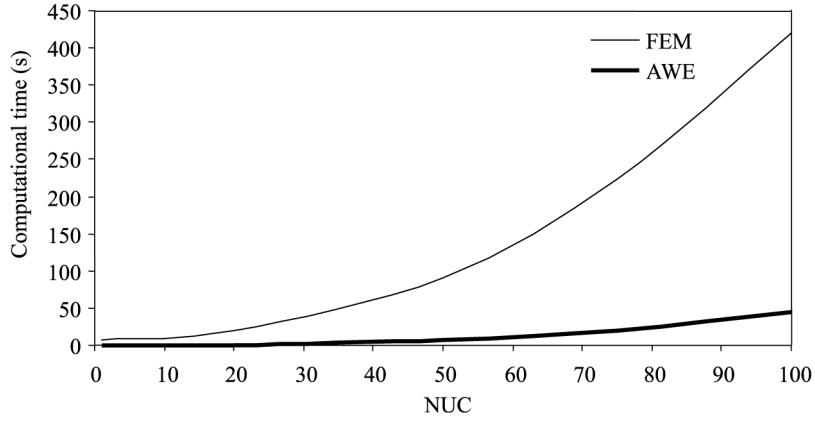

Figure 13.
Comparison of computational time for FEM and AWE scheme to reach steady-state value for loss = 0, $\tilde{Q} = 1$ and $M = 0.55$

method and the results thus obtained are compared with those by FEM. The following conclusions are drawn.

(1) The single unit cell as the representative of the stack is only valid either if there are no heat losses from the top and bottom surfaces of the stack or there are more than 100 unit cells in the triple stack.

(2) New results for triple stack cold plates in terms of the steady-state maximum temperature of the stack obtained under different heat loadings for various values of M are presented. For higher values of M, NUC = 50 is sufficient for the analysis to get the maximum temperature.

(3) New results for the triple stack cold plate in terms of the steady-state temperature distribution along the left and right exterior plates for heat losses from the top surface being different from the bottom surface for a particular heat loading and a particular value of M are also presented. The trends obtained are expected.

(4) The time taken to reach the steady-state is shorter as the heat losses at the top and bottom surface increase. Also, as the heat loading increases, the time taken to reach the steady-state is longer. Similar trend is observed as the NUC increases. However, as M increases, the time taken to reach the steady-state reduces considerably.

(5) There is a good agreement between the transient results obtained by the fast transient AWE method and the finite element method applied to the triple stack with different operating conditions. However, the time taken to analyse the transient performance by AWE scheme is considerably shorter.

References

Beh, S.L., Quadir, G.A. and Seetharamu, K.N. (2001), "A transient finite element analysis of single, double and triple stack cold plates", *International Journal of Heat Exchangers*, Vol. II No. 2, pp. 179-200.

Kraus, A.D. and Pieper, R.J. (1995), "Cold plates with asymmetric heat loading, Part II – The double stack", *Advances in Electronic Packaging*, EEP-10-2, ASME, NY, pp. 871-8.

Kraus, A.D., Snider, A.D. and Dty, L.F. (1978), "An efficient algorithm for evaluating arrays of extended surfaces", *ASME Journal of Heat Transfer*, Vol. 100, pp. 288-93.

Lewis, R.W., Morgan, K., Thomas, H.R. and Seetharamu, K.N. (1996), *Finite Element Method in Heat Transfer Analysis*, Wiley, New York, NY.

Mikhailov, M.D. and Ozisik, M.N. (1981), *Heat Exchangers: Thermal-Hydraulic Fundamentals and Design in Finite Element Analysis of Heat Exchangers*, McGraw-Hill Book Company, New York, NY.

Pieper, R.J. and Kraus, A.D. (1995), "Cold plates with asymmetric heat loading, Part I – The single stack", *Advances in Electronic Packaging*, EEP-10-2, ASME, NY, pp. 865-70.

Pieper, R.J. and Kraus, A.D. (1998), "Performance analysis of double stack cold plates covering all conditions of asymmetric heat loading", *ASME Journal of Electronic Packaging*, Vol. 20, pp. 296-301.

Quadir, G.A., Beh, S.L., Seetharamu, K.N. and Hassan, A.Y. (2002), "Steady state finite element analysis of a single stack cold plate with heat losses", *ASEAN Journal on Science and Technology for Development*, Vol. 19 No. 1, pp. 77-90.

Quadir, G.A., Beh, S.L., Seetharamu, K.N. and Hassan, A.Y. (2003), "Steady state finite element analysis of a double stack cold plate with heat losses", *Heat and Mass Transfer*, Vol. 39, pp. 519-28.

Segerlind, L.J. (1984), *Applied Finite Element Methods*, Wiley, New York, NY.

Further reading

Pieper, R.J. and Kraus, A.D. (1997), "A transient analysis of heat transfer in double stack cold plates", *Proc. 29th Southeastern Symposium on System Theory (SSST)*, Cookeville, TN, pp. 348-52.